Journal of Engineering and Development

www.jead.org
Vol. 19, No. 06, November 2015
ISSN 1813-7822

QUANTUM EFFICIENCY OF A p-υ-n Si PHOTODETECTOR

Dr.Muneer Aboud Hashem, Mohammad Shihab Ahmmed

1) Assist. Prof., Electrical Eng. Department, Al-Mustansiryah University, Baghdad, Iraq.
2) M. Sc., in Electronic and Communication, Electrical Eng. Department, Al-Mustansiryah University, Baghdad, Iraq.

(Received: 13/10/2014; Accepted: 19/4/2015)

Abstract: The quantum efficiency of a silicon p-υ-n photodetector is present. The analysis to obtain the quantum efficiency takes a uniform doping concentration in each layer into consideration. The theoretical treatment aims to investigate the effect of device parameters on the efficiency. Three different cases of the incident light wavelengths have been considered; short wavelengths, medium wavelengths, and long wavelengths. There is no wavelength range between them, but when the most of the incident light (about 63% or more) absorbed near the surface, it is called short wavelength, and when most of the light absorbed in υ-layer, it is called medium wavelength else called long wavelength.A high quantum efficiency at the wavelength of interest, combine with its low operating voltage and capability, make this detector a promising for use in communication systems and computer interconnections.High speed silicon p-υ-n photodetector operates at $700\,\text{nm}$ wavelength is reported. By using a reverse bias voltage to control υ-layer width, a high quantum efficiency of 80% is attained corresponding to υ-layer width of $5.36\,\mu\text{m}$ and biasing voltage of $2.182\,\text{V}$ .The results showed that the quantum efficiency is directly proportional to the width of the υ-layer and biasing voltage. The results are achieved with the aid of MATLAB programming tool version $8.1.0.604\left(R2013a\right)$.

Keywords: *quantum efficiency, photodetector, p-υ-n photodiode.*

الكفاءة الكمية للكاشف الضوئي p-υ-n سليكون

الخلاصة: تم تقديم الكفاءة الكمية للكاشف الضوئي المصنوع من السليكون ذو التركيب p-υ-n . أن تحليل كفاءة الكم المذكورة تعتبر تركيز الشوائب منتظم في كل طبقة. تهدف المعالجة النظرية لدراسة تأثير باراميترات الجهاز على الكفاءة. وقد تم اعتبار ثلاث حالات مختلفة من الطول الموجي للضوء الساقط، اطوال موجية قصيرة، اطوال موجية متوسطة واطوال موجية طويلة. لايوجد مدى محدد بين تلك الاطوال الموجية، ولكن عندما معظم الضوء الساقط (حوالي 63% او اكثر) يمتص بالقرب من السطح، يسمى طول موجي قصير، وعندما معظم الضوء الساقط يمتص بطبقة υ، يسمى الطول الموجي المتوسط والا فيسمى الطول الموجي الطويل.ان الكفاءة الكمية العالية عند طول موجي معين بالارتباط مع الفولتية المطبقة وقابلية تشغيلها المنخفضة، يجعل هذاالكاشف واعد للاستخدام في نظم الاتصالات ووصلات الكومبيوتر.الكاشف الضوئي p-υ-n سليكون ذو السرعة العالية عند الطول الموجي ٧٠٠ نانومتر قد تم ذكره. باستخدام التحيز العكسي للسيطرة على عرض طبقة υ، تم الوصول الى كفاءة كم عالية بحدود 80% عندما كان عرض طبقة υ هو 5.36 مايكرومتر وفولتية الانحياز 2.182 فولت.اظهرت النتائج ان كفاءة الكم تتناسب طرديا عرض طبقة υ وفولتية الانحياز. ان النتائج تم انجازها بالاستعانة باداة البرمجة MATLAB النسخة $8.1.0.604$.

**Corresponding Author* muneraboud@yahoo.com

1. Introduction

A high quantum efficiency (Q.E) value means a high amount of incident light have been absorbed. The ideal quantum efficiency is unity. The lessening is due to the current loss by recombination, incomplete absorption, reflection, etc.

The incident photon with an energy hf (where h is Plank's constant and f is the frequency of incident light) $> E_g$ (where E_g is energy of bandgap, related with bandgap wavelength λ_g) excites an electron from the valence band to the conduction band and so creating an electron-hole pair (EHP) [1].

When the photodiode reverse biased, it operates as a photodetector. The photodetector can not detect all light wavelengths, so the detection of the light at certain wavelength requires a certain design. The ability of the photodetector to detect the light is called responsivity.

The p-υ-n photodiode structure is shown in "Fig. 1", which consists of a large thickness of lightly negative doped υ-layer sandwich between a p- and n-layers. A positive charge is created in υ-layer as ionized donors.

In 1999, Schaub, J.D. et al., designated a resonant cavity enhancement Si photodiode grown by merged epitaxial lateral overgrowth (MELO), who carried out a bandwidth of 34 GHz and a peak quantum efficiency of 42% at a wavelength of 704 nm [2]. In 2011, Habibpoor, A., utilized a one dimensional (1-D) simulation program based on the drift-diffusion model and Discrete Fourier Transform (DFT) is developed. The program numerically solves the time-dependent continuity equations for electrons and holes in a semiconductor device. The model simulates carrier concentrations and the impulse response of a gallium arsenide metal-semiconductor-metal photodetector at a constant bias voltage. The simulation showed that for a smaller value of carrier lifetime, the response fall time decreases without significantly reducing the quantum efficiency of the device [3].

As shown from "Fig. 1" w_p represents bulk p-side width, x_p is the depletion width provided by p-side, w_υ is the width of υ-layer, x_n is the depletion width provided by n-side, w is the depletion width, and w_n is bulk n-side width.

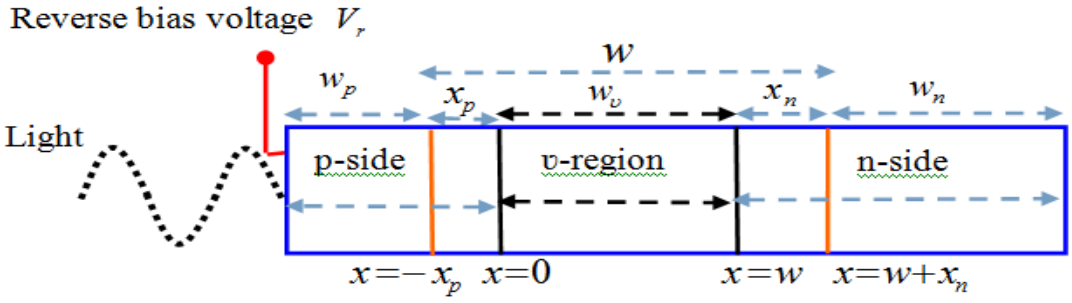

Figure 1. p-υ-n photodiode structure.

The wavelength of incident light λ is given by [4],

$$\lambda = c/f \quad (1)$$

where c is light velocity.

The generation rate of EHPs $G(x)$ is given by [5],

$$G(x) = -\frac{d\Phi(x)}{dx} = \alpha\Phi(x) = \alpha\Phi_o e^{-\alpha.x} \quad (2)$$

where Φ is incident light density, $\Phi_o = \Phi(x=0)$, α is absorption coefficient and it is a function of incident light wavelength.

2. p-υ-n Photodetector Under Biasing

The reverse biasing voltage determines the equation of the depletion layer width w. If a large enough reverse bias voltage applied to the detector and fully deplete the bulk of charge carriers in the υ-layer, there will be a non-zero electric field extending all the way across it due to the ionized donor atoms. The voltage at which this happens is referred to as the punch-through voltage V_{PT}.

When applied reverse bias voltage equals to punch-through voltage $(V_r = V_{PT})$, in this case $x_p = x_n = 0$, then $w = w_\upsilon$. The punch-through voltage is given by [6].

$$V_{PT} \approx \frac{qN_d}{2\varepsilon} w_\upsilon^2 \quad (3)$$

where q is particle charge constant, N_d is donor doping concentration in υ-layer (about 10^{13} cm^{-3}), and ε is permittivity.

3. Carrier Density Distribution

The flow of electrons in the p-side is governed by [7],

$$\frac{\partial n_p(x,t)}{\partial t} = D_n \frac{\partial^2 n_p(x,t)}{\partial x^2} + G_n(x,t) - \left[\frac{n_p(x,t) - n_{po}}{\tau_n}\right] \quad (4a)$$

where $n_p(x,t)$ is electrons concentration under illumination in the p-side, D_n is an electrons diffusion coefficient, $G_n(x,t)$ is an electrons generation rate, n_{po} is an electrons concentration under equilibrium, and τ_n is electrons lifetime.

The flow of holes in the n-side is governed by [8].

$$\frac{\partial p_n(x,t)}{\partial t} = D_p \frac{\partial^2 p_n(x,t)}{\partial x^2} + G_p(x,t) - \left[\frac{p_n(x,t) - p_{no}}{\tau_p} \right] \quad (4b)$$

where $p_n(x,t)$ is holes concentration under illumination in the n-side, D_p is holes diffusion coefficient, $G_p(x,t)$ is holes generation rate, p_{no} is holes concentration under equilibrium, and τ_p is holes lifetime.

Carriers diffusion coefficients are given by,

$$D_n = L_n^2 / \tau_n \quad (5a)$$

$$D_p = L_p^2 / \tau_p \quad (5b)$$

where L_n is electron diffusion length, and L_p is hole diffusion length,

4. Current of Vertical Illuminated p-υ-n Photodetector

The current generated inside υ-layer is called drift current and the current generated outside υ-layer is called diffusion current. The one-dimensional diffusion current density, for electrons, $J_{diff,n}$, and for holes, $J_{diff,p}$, are [9]:

$$J_{diff,n}(x) = qD_n \frac{dn_p(x)}{dx} \quad \text{p-side} \quad (6a)$$

and

$$J_{diff,p}(x) = -qD_p \frac{dp_n(x)}{dx} \quad \text{n-side} \quad (6b)$$

4.1. Diffusion Current

i) p-side Diffusion Current

The flow of minority carrier density (electrons) in the bulk p-side is determined by "(4a)". At steady state, $n_p(x,t) = n_p(x)$, and $G_n(x,t) = G_n(x)$. Using "(4a)" with "(2)" gives,

$$\frac{\partial^2 n_p(x)}{\partial x^2} - \left[\frac{n_p(x) - n_{po}}{L_n^2}\right] = -\frac{\Phi_o \alpha e^{-\alpha x}}{D_n} \tag{7}$$

The general solution to "(7)" is a sum of homogenous solution $n_h(x)$ and particular solution $n_{Pa}(x)$.

$$n_p(x) = n_h(x) + n_{pa}(x) \tag{8}$$

The homogenous solution is,

$$n_h(x) = Ce^{x/L_n} + De^{-x/L_n} \tag{9}$$

and the particular solution is,

$$n_{pa}(x) = A + Be^{-\alpha x} \tag{10}$$

From "(10)", $n'_{Pa}(x) = -\alpha Be^{-\alpha x}$, $n''_{Pa}(x) = \alpha^2 Be^{-\alpha x}$, substituting $n_{Pa}(x)$, $n'_{Pa}(x)$ and $n''_{Pa}(x)$ into "(7)" yields,

$A = n_{po}$ and $B = \dfrac{\Phi_o \alpha L_n^2}{D_n\left(1 - \alpha^2 L_n^2\right)}$.

Substituting A and B into "(10)" gives,

$$n_{pa}(x) = n_{po} + \frac{\Phi_o \alpha L_n^2}{D_n\left(1 - \alpha^2 L_n^2\right)} e^{-\alpha x} \tag{11}$$

and substituting "(9)" and "(10)" into "(8)", the minority carrier distribution is given by,

$$n_p(x) = Ce^{x/L_n} + De^{-x/L_n} + n_{po} + \frac{\Phi_o \alpha L_n^2}{D_n\left(1 - \alpha^2 L_n^2\right)} e^{-\alpha x} \tag{12}$$

and using the first boundary condition $n_p(x = 0) = n_{po}$,

$$0 = C + D + C_1 \tag{13a}$$

where $C_1 = \dfrac{\Phi_o \alpha L_n^2}{D_n\left(1 - \alpha^2 L_n^2\right)}$.

Using the second boundary condition $n_p(x = w_p) = 0$,

,

$$0 = Ce^{w_p/L_n} + De^{-w_p/L_n} + n_{po} + C_1 e^{-\alpha w_p} \quad (13b)$$

From "(13a)" and "(13b)",

$$C = \frac{\left[C_1\left(e^{-w_p/L_n} - e^{-\alpha w_p}\right) - n_{po}\right]}{2\sinh\left(w_p/L_n\right)} \quad \text{and} \quad D = \frac{\left[C_1\left(-e^{w_p/L_n} + e^{-\alpha w_p}\right) - n_{po}\right]}{2\sinh\left(w_p/L_n\right)}$$

Substituting C and D into "(12)" gives,

$$n_p(x) = n_{po} + C_1 e^{-\alpha w_p} + \frac{-n_{po}\sinh\left(x/L_n\right) + C_1\sinh\left(\left(x - w_p\right)/L_n\right) - C_1 e^{-\alpha w_p}\sinh\left(x/L_n\right)}{\sinh\left(w_p/L_n\right)} \quad (14a)$$

$$\left.\frac{dn_p(x)}{dx}\right|_{w_p} = -\alpha C_1 e^{-\alpha w_p} + \frac{C_1\left[1 - e^{-\alpha w_p}\cosh\left(w_p/L_n\right)\right]}{L_n\sinh\left(w_p/L_n\right)} - \frac{n_{po}}{L_n}\frac{\cosh\left(w_p/L_n\right)}{\sinh\left(w_p/L_n\right)} \quad (14b)$$

Substituting "(14b)" into "(6a)",

$$J_{diff,n}\left(w_p\right) = qD_n\left[-\alpha C_1 e^{-\alpha w_p} + \frac{C_1\left[1 - e^{-\alpha w_p}\cosh\left(w_p/L_n\right)\right]}{L_n\sinh\left(w_p/L_n\right)} - \frac{n_{po}}{L_n}\coth\left(w_p/L_n\right)\right] \quad (15a)$$

The term in "(15a)" that contains Φ_o represent diffusion photocurrent in the p-side $J_{diff,ph,n}$ so,

$$J_{diff,ph,n}\left(w_p\right) = qD_n C_1\left[-\alpha e^{-\alpha w_p} + \frac{\left[1 - e^{-\alpha w_p}\cosh\left(w_p/L_n\right)\right]}{L_n\sinh\left(w_p/L_n\right)}\right] \quad (15b)$$

ii) n-side Diffusion Current

The flow of minority carrier density (holes) in the bulk n-side is determined by "(4b)". At steady state, $p_n(x,t) = p_n(x)$, and $G_p(x,t) = G_p(x)$. Using "(4b)" with "(2)" gives,

$$\frac{\partial^2 p_n(x)}{\partial x^2} - \left[\frac{p_n(x) - p_{no}}{L_p^2} \right] = -\frac{\Phi_o \alpha e^{-\alpha x}}{D_p} \tag{16}$$

The procedure used to find $n_p(x)$ is the same to find $p_n(x)$ but the boundary conditions are, $p_n(x=\infty) = p_{no}$ and $p_n(x = w_\upsilon + w_p) = 0$.

The holes distribution in the n-side neutral region is,

$$p_n(x) = p_{no} - \left[p_{no} + C_1 e^{-\alpha(w_\upsilon + w_p)} \right] e^{(w_\upsilon + w_p - x)/L_p} + C_1 e^{-\alpha x} \tag{17a}$$

where $C_1 = \dfrac{\Phi_o \alpha L_p^2}{D_p(1 - \alpha^2 L_p^2)}$.

From "(17a)",

$$\frac{dp_n(x)}{dx} = \frac{1}{L_p}\left[p_{no} + C_1 e^{-\alpha(w_\upsilon + w_p)} \right] e^{(w_\upsilon + w_p - x)/L_p} - \alpha C_1 e^{-\alpha x} \tag{17b}$$

Substituting "(17b)" into "(6b)" yields,

$$J_{diff,p}(w_\upsilon + w_p) = \frac{-qp_{no}D_p}{L_p} - \frac{q\Phi_0 \alpha L_p}{1 + \alpha L_p} e^{-\alpha(w_\upsilon + w_p)} \tag{18a}$$

The term in "(18a)" that contains Φ_o represent diffusion photocurrent in the n-side $J_{diff,ph,p}$ so,

$$J_{diff,ph,p} = -\frac{q\Phi_0 \alpha L_p}{1 + \alpha L_p} e^{-\alpha(w_\upsilon + w_p)} \tag{18b}$$

4.2. Drift Current

The drift current density due to absorbed light inside υ-layer is,

$$J_{drift,ph,w} = -q\int_{w_p}^{w_p + w_\upsilon} G(x)dx = -q\Phi_o e^{-\alpha w_p}\left(1 - e^{-\alpha w_\upsilon}\right) \tag{19}$$

5. Quantum Efficiency Analysis

There are essentially three types of the photogeneration process that can participate to the absorbed photocurrent I_{ph}, due to the wavelength of the incident light.

5.1. Short Wavelengths

In this case the absorption depth $(1/\alpha)$ is less than the width w_p. The photogeneration takes place mainly within w_p. The total generation photocurrent equals to the electrons photocurrent in the p-side as shown in "Fig. 2", so the quantum efficiency η is given by,

$$\eta = \frac{\left|J_{diff,ph,n}\right|/q}{\Phi_o} = \frac{\alpha L_n^2}{1-\alpha^2 L_n^2}\left[-\alpha e^{-\alpha w_p} + \frac{\left[1-e^{-\alpha w_p}\cosh\left(w_p/L_n\right)\right]}{L_n \sinh\left(w_p/L_n\right)}\right] \tag{20}$$

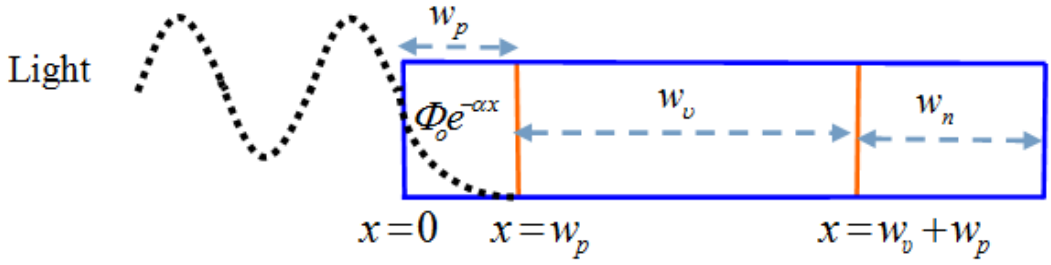

Figure 2. Absorption due to short wavelengths.

5.2. Medium Wavelengths

The absorption depth in this case is comparable with $w_p + w_\upsilon$. Significant photogeneration now takes place within υ-layer. The total generation photocurrent equals to the electron photocurrent in the p-side plus drift photocurrent in the υ-layer as shown in "Fig. 3', so the quantum efficiency is given by,

$$\eta = \frac{\left|J_{diff,ph,n} + J_{drift,ph,w}\right|/q}{\Phi_o} = \left[e^{-\alpha w_p} + \frac{\left[1-e^{-\alpha w_p}\cosh\left(w_p/L_n\right)\right]}{\alpha L_n \sinh\left(w_p/L_n\right)}\right] + e^{-\alpha w_p}\left(1-e^{-\alpha\left(w_\upsilon + w_p\right)}\right) \tag{21}$$

by ensuring $\alpha L_n >> 1$,

$$\eta \approx \left(1-e^{-\alpha w_\upsilon}\right) \tag{22}$$

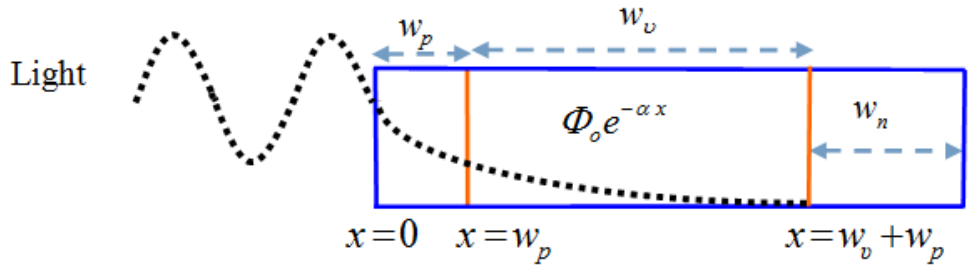

Figure 3. Absorption due to medium wavelengths.

5.3. Long Wavelengths

In this situation the absorption depth is longer than $w_p + w_\upsilon$, as shown in "Fig. 4". The total generation photocurrent equals to the electron photocurrent in the p-side plus drift photocurrent in the υ-layer plus hole photocurrent in the n-side. The quantum efficiency is,

$$\eta = \frac{\left|J_{diff,ph,n} + J_{drift,ph,w} + J_{diff,ph,p}\right|/q}{\Phi_o} = \left[e^{-\alpha w_p} - \frac{\left[1-e^{-\alpha w_p}\cosh\left(w_p/L_n\right)\right]}{\alpha L_n \sinh\left(w_p/L_n\right)}\right] + e^{-\alpha w_p} \times\left(1-e^{-\alpha\left(w_\upsilon+w_p\right)}\right)e^{-\alpha w_p} + \frac{\alpha L_p e^{-\alpha\left(w_\upsilon+w_p\right)}}{1+\alpha L_p} \quad (23)$$

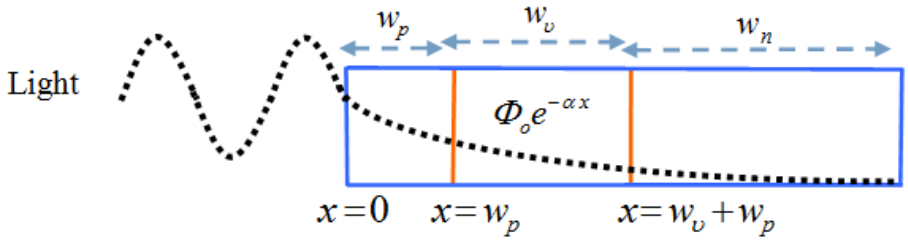

Figure 4. Absorption due to long wavelengths.

The flowchart in "Fig. 5" shows the steps of the analysis to obtain the quantum efficiency at different wavelengths of incident light.

6. Maximum Quantum Efficiency

The relation between quantum efficiency and wavelength is given by [10],

$$\eta = 1.24\frac{\Re(\lambda)}{\lambda(\mu m)} \quad (24)$$

where $\Re$ is responsivity of the device.

From "(24)", the maximum quantum efficiency can be obtained by differentiation responsivity with respect to λ, then setting the derivative to zero, this gives a line through the origin that is a tangent to the $\Re$ versus λ curve. This tangential point is X as shown in "Fig. 6". At this point, $\lambda = 700\,\text{nm}$ and $\Re = 0.45\,\text{A/W}$, substituting λ and $\Re$ into "(24)" yields [4],

$$\eta \approx 0.8 \text{ or } 80\% \tag{25}$$

7. Requirements for Maximum Q.E

As demonstrated in section (5.2) the best quantum efficiency can be obtained for medium wavelengths, since the diffusion terms suppressed, so the best design is by making the absorption depth is comparable to $w_p + w_\upsilon$.

Substituting "(22)" into "(25)" yields,

$$-1.609 = -\alpha w_\upsilon \tag{26}$$

At $\lambda = 700\,\text{nm}$ the absorption coefficient is $3\times10^3\ \text{cm}^{-1}$, then from "(26)" $w_\upsilon \approx 5.36\,\mu\text{m}$, this value represents υ-layer width required to get full absorption of incident light.

Using "(1)", when $\lambda = 700\,\text{nm}$ then $f = 428.572\times10^{12}\ \text{Hz}$, and photon energy is $E_{ph} = 1.77\,\text{eV}$, this energy is greater than the direct bandgap energy of silicon, so direct absorption is obtained.

At $w_\upsilon = 1/\alpha$, the quantum efficiency is,

$$\eta = \left(1 - e^{-\alpha w_\upsilon}\right) = \left(1 - e^{-1}\right) = 0.628 \approx 63\% \tag{27}$$

8. Results and Discussion

The punch-through voltage and quantum efficiency as a function of υ-layer width are shown in "Fig. 7" and "Fig. 8", respectively. The reported quantum efficiency is 63% at υ-layer width of $0.33\,\mu\text{m}$, and is 80% at υ-layer width of $5.36\,\mu\text{m}$. It can be seen that as the width of υ-layer increases the punch-through voltage is increased. The quantum efficiency increases with increasing in υ-layer width. The quantum efficiency can be improved by making the width of υ-layer width as much as possible, since this layer is completely depleted of carriers.

A maximum value of the quantum efficiency can be reached for the case of medium wavelength of detection, where the wavelength of the incident light is not small for maximum absorption near the surface to occur that is lead to reduce the quantum efficiency as a result of recombination. Also the wavelength is not high, where the light penetrates more deeply as a result of very small absorption.

The practical curve between resposivity and wavelength is shown in "Fig. 6". From "(24)" the ideal curves of responsivity versus wavelength are shown in "Fig. 9". This figure is not a practical one, since as wavelength increases the absorption coefficient decreases, and then the incident light enters deeply into the detector and this requires a large υ-later width to get full absorption.

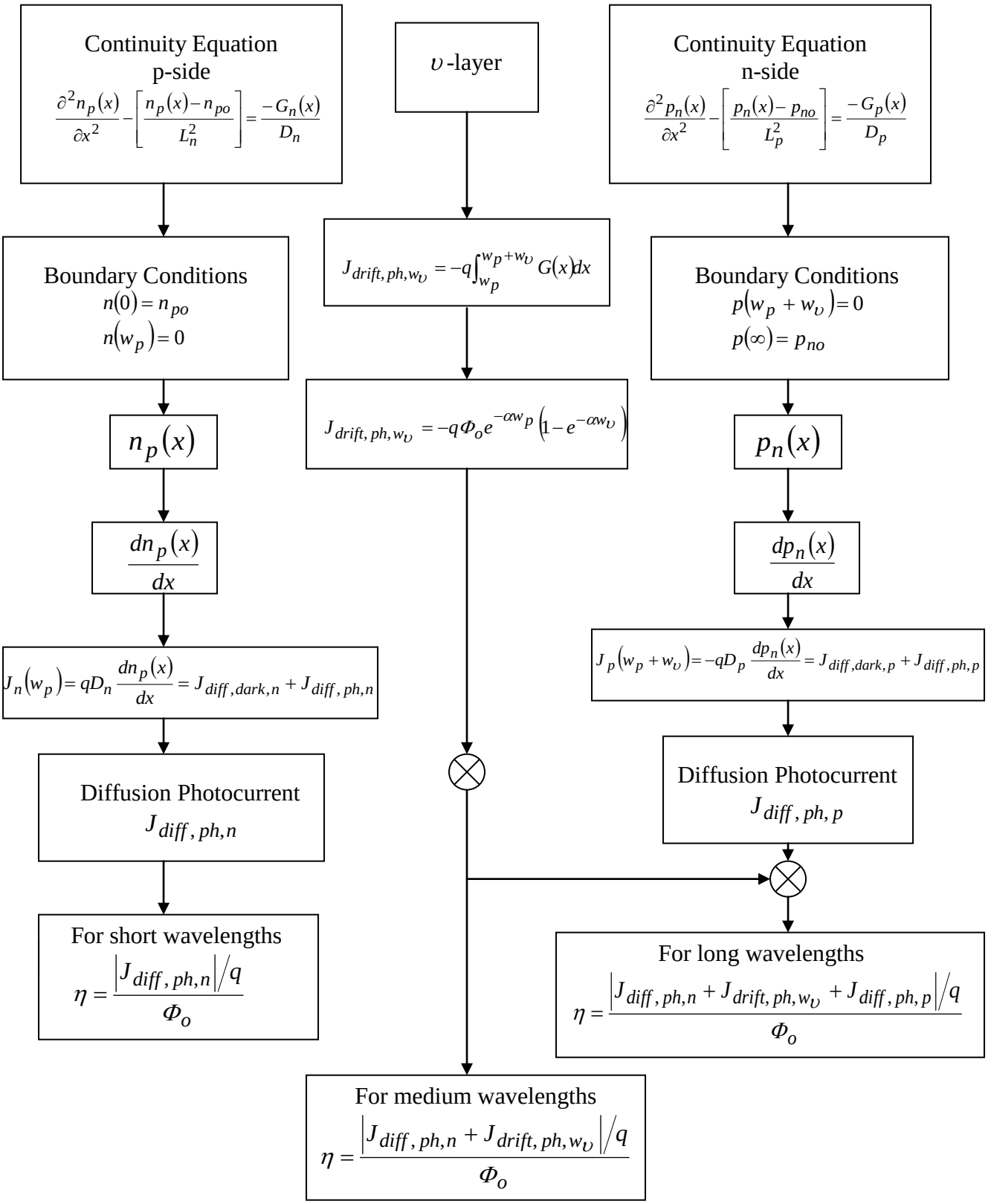

Figure 5. Flowchart showing steps to obtain quantum efficiency.

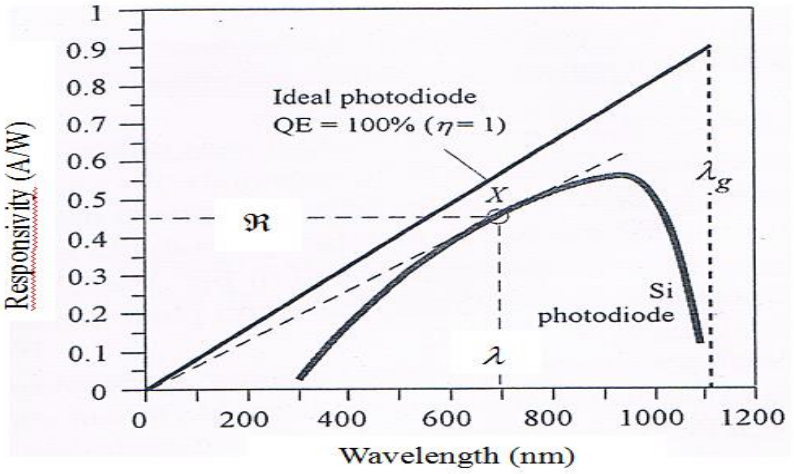

Figure 6. Responsivity versus wavelength

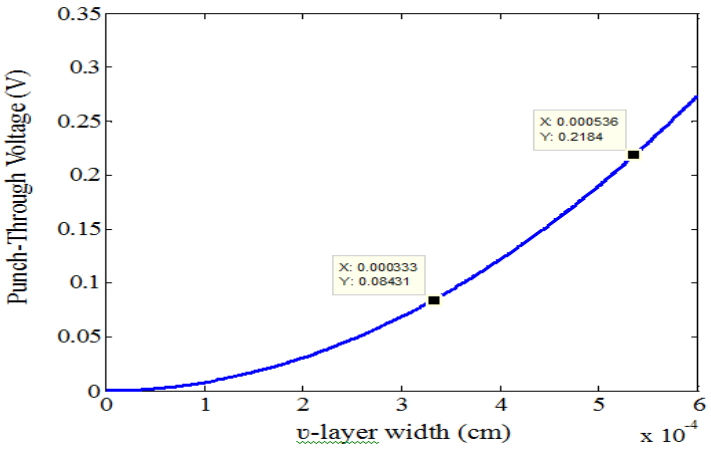

Figure 7. Punch-through voltage versus υ-layer width

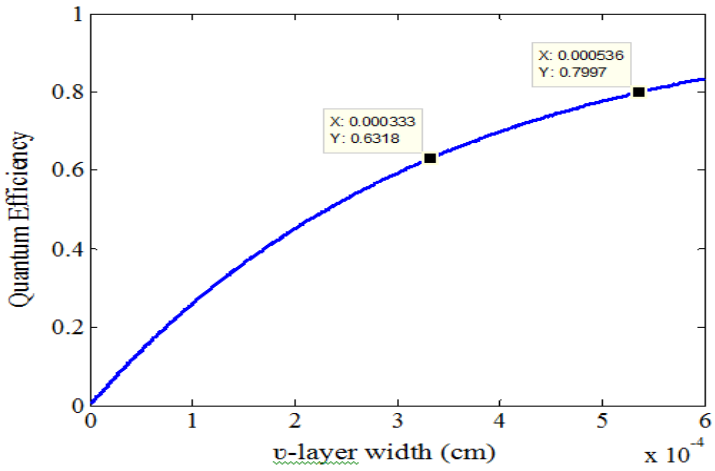

Figure 8. Quantum efficiency versus υ-layer width

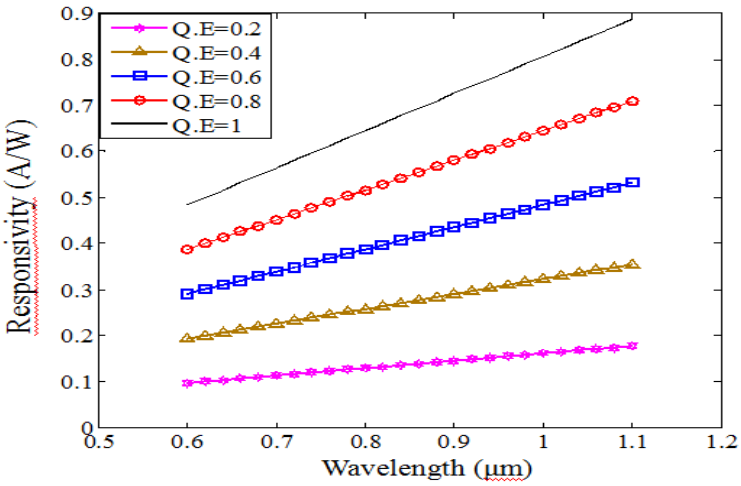

Figure 9. Ideal curve for responsivity versus wavelength for different quantum efficiency values

9. Conclusions

The analysis of p-υ-n photodetector was accomplished. The following points are concluded;

i- At low frequency of incident light the p-υ-n photodetector can operate with long wavelengths (less photon energy).

ii- At high frequency, the absorption coefficient be high, then the light absorbed near the surface, the recombination rate near the surface is very high due to recombination centers near it, then the quantum efficiency be low. If the light frequency is low, then the light enters deeply into the sample, and if the condition $E_{ph} > E_g$ does not exist, then the detector is as transparent layer (the light not absorbed by the detector) and the quantum efficiency is low.

iii- At a υ-layer width of $5.36\,\mu$m, the low biasing voltage required about $27.5\,$V, that is because the υ-layer in p-υ-n photodetector is already depleted.

iv- In the photodetector design, the choosing of υ-layer width, depending on the absorption coefficient, which in turn function of wavelength of incident light.

v- Since a high width of υ-layer leads to high quantum efficiency, this leads also to better RC time constant according to low value of junction capacitance. This increases the transit time of carriers to pass through υ-layer, and affect the bandwidth capability of the device. A trade-off between the mentioned parameters should be taken into consideration for optimum device operation.

References

1. Green, M.A. and Keevers, M.J. (1995). "Optical properties of intrinsic silicon at $300\,$K". Progress in Photovoltaics, Research and Applications, Vol. 3, No. 3, pp.189-192.
2. Schaub, J.D, Li, R., Schow, C.L. and Campbell, J.C. (1999). "Resonant-cavity-enhanced high-speed Si photodiode grown by epitaxial lateral overgrowth". IEEE Photonics Technology Letters, Vol.11, No.12, pp. 1647-1649.

3. Habibpoor, A. and Mashayekhi, H.R. (2011). "Numerical modeling of the transient response of metal-semiconductor-metal photodetector using discrete Fourier transform". Journal of Physics, Vol. 286, No.1, pp. 1-6.
4. Kasap, S.O. (2012). "Optoelectronics and Photonis". 2nd Ed., Prentice Hall.
5. Suzuki, G., Konno, K. Navarro, D., Sadachika, N., Mizukane, Y., Matsushima, O. and Miura-Mattausch, M. (2005). "Time-domain-based modeling of carrier transport in lateral pin photodiode,". International conference on IEEE, Simulation of Semiconductor Processes and Devices, pp. 107-110.
6. Colinge, J.P. and Colinge, C.A. (2005). "Physics of Semiconductor Devices". Springer,
7. Zeghbroeck, B.V. (2001). "Principles of Semiconductor Devices". Prentice-Hall.
8. Jou, J.J., Liu, C.K., Hsiao, C.M., Lin, H.H. and Lee, H.C. (2002). "Time-delay circuit model of high-speed p-i-n photodiodes". IEEE Photonics Technology Letters, Vol.14, No. 4, pp. 525-527.
9. Anderson, B.L. and Anderson, R.L. (2004). "Fundamentals of Semiconductor Devices" McGraw-Hill.
10. Yu, J., Shan, C.X., Qiao, Q., Xie, X.H., Wang, S.P., Zhang, Z.Z. and Shen, D.Z. (2012) "Enhanced responsivity of photodetectors realized via impact ionization". Sensors, Vol. 12, No.2, pp. 1280-1287.